PHYSICAL REVIEW B **82**, 081412(R) (2010)

Crystal-induced effects at crystal/amorphous interfaces: The case of Si_3N_4/SiO_2

Weronika Walkosz,[1] Robert F. Klie,[1] Serdar Öğüt,[1] Biljana Mikijelj,[2] Stephen J. Pennycook,[3,4] Sokrates T. Pantelides,[4,3] and Juan C. Idrobo[1,4,3]

[1]*Department of Physics, University of Illinois at Chicago, Chicago, Illinois 60607, USA*
[2]*Ceradyne, Inc., Costa Mesa, California 92626, USA*
[3]*Materials Science and Technology Division, Oak Ridge National Laboratory, Oak Ridge, Tennessee 37831, USA*
[4]*Department of Physics and Astronomy, Vanderbilt University, Nashville, Tennessee 37235, USA*

(Received 2 July 2010; revised manuscript received 10 August 2010; published 25 August 2010)

We reveal the presence of atomic short-range ordering at the interface between crystalline β-Si_3N_4 and amorphous SiO_2 using aberration-corrected scanning transmission electron microscopy. We show that the first atomic layers of the amorphous SiO_2 film reconstruct taking on the crystalline form of Si_3N_4. Furthermore, we find that there is a nonuniform interatomic mixing of oxygen and nitrogen at different atomic sites at the interface. The work provides a direct look at the atomic structure of crystal/amorphous interfaces composed of light elements.

DOI: 10.1103/PhysRevB.82.081412 PACS number(s): 68.35.Rh, 68.37.Ma, 68.35.bj

A vast range of technological materials rely on crystal/amorphous interfaces for their performance. In Si_3N_4 structural ceramics, the overall mechanical and thermal properties are controlled by the atomic and electronic structures at the interface between the ceramic grains and the amorphous intergranular films (IGFs) formed by various sintering additives.[1–7] The very small thickness (~1–2 nm) of the IGFs, however, poses difficulties for detailed identification of surface relaxations and reconstructions, interatomic mixing, as well as possible partial ordering at the interface. Some evidence of the latter has emerged, but all so far have involved heavy cations.[8–15] Key knowledge, however, has been missing concerning the position of light atoms, without which it is not possible to obtain complete understanding of the interfaces. To date, most of the work on the films composed of light atoms and their interfaces in Si_3N_4 has focused on atomistic simulations and *ab initio* modeling.[16–20]

In this Rapid Communication, we reveal the presence of atomic short-range ordering at the interface between crystalline β-Si_3N_4 and amorphous SiO_2 using aberration-corrected scanning transmission electron microscopy (STEM). We show that the first atomic layers of the amorphous SiO_2 film reconstruct in the vicinity of the interface to adopt the crystalline form of Si_3N_4. Furthermore, we find that there is a nonuniform interatomic mixing of oxygen and nitrogen at different atomic sites at the interface. The results show that the compositional and spatial identification of crystal/amorphous interfaces can be now obtained at the atomic scale. This information will enable realistic investigation of electronic and structural properties of various interfaces through atomistic simulations, bringing opportunities to fine-tune compositions with improved properties for devices in general.

We have utilized three different imaging techniques in STEM, i.e., bright-field (BF), annular BF (ABF), and Z-contrast imaging (also known as high angle-annular dark field or HA-ADF imaging), as well as electron energy loss spectroscopy (EELS) at different electron beam voltages to characterize the interface of Si_3N_4 $(10\bar{1}0)$ and the amorphous SiO_2 IGF at the atomic scale. The ABF images were acquired with a collection semiangle from 11 to 22 mrad, while the BF images at 300 kV were acquired with a collection semiangle of 35 mrad. The Z-contrast images at 80, 120, and 300 kV were acquired with convergence semiangles of 30, 22, and 23 mrad and inner detector semi-angles of 90 mrad, 90 mrad, and 84 mrad, respectively. For EEL spectroscopy at 80 and 300 kV, a convergence semiangle of 35 and 23 mrad and a collection semiangle of 64 and 35 mrad were used. The sample used in this work was consolidated by uniaxial hot pressing of a finely mixed and dispersed 95% α-Si_3N_4 (SSA of 11 m^2/g) powder with pure SiO_2 (SSA 4 m^2/g, 1000 total ppm metal impurities) powder in a 71/29 weight ratio. The grains selected for imaging and spectroscopic measurements were those displaying definite and sharp edges, as these interfaces were observed to exhibit no significant contrast variation in the vicinity of the Si_3N_4 surface, terminated with open rings, when viewed edge-on with respect to the electron beam. This ensured that the observed features at the interface with the intergranular film were not due to the surface steps often formed in Si_3N_4 grains.

Figures 1(a) and 1(b) show a Z-contrast image and an ABF image of the interface acquired simultaneously in an aberration corrected JEOL ARM 200F operated at 120 kV. The characteristic hexagonal rings of the ceramic in the [0001] orientation formed by the Si and N atoms are clearly visible in the images. The dotted lines mark the termination of the Si_3N_4 surface with the terminating open rings along the $(10\bar{1}0)$ direction. These open structures have been consistently observed at the Si_3N_4/rare-earth oxides and Si_3N_4/SiO_2 interfaces.[8–15] The ABF image [Fig. 1(b)] reveals significant additional information about the interface structure compared to the Z-contrast image. It clearly shows that crystalline order is also present away from the interface, deeper into the amorphous SiO_2 region, as shown by the appearance of dark spots above the dotted line in Fig. 1(b). However, at 120 kV individual silicon and nitrogen atomic columns cannot be clearly resolved.

To improve the image resolution, we have repeated the experiments at higher voltages. Figures 1(c) and 1(d) show the acquired Z-contrast and BF images, respectively, at 300

 ©2010 The American Physical Society

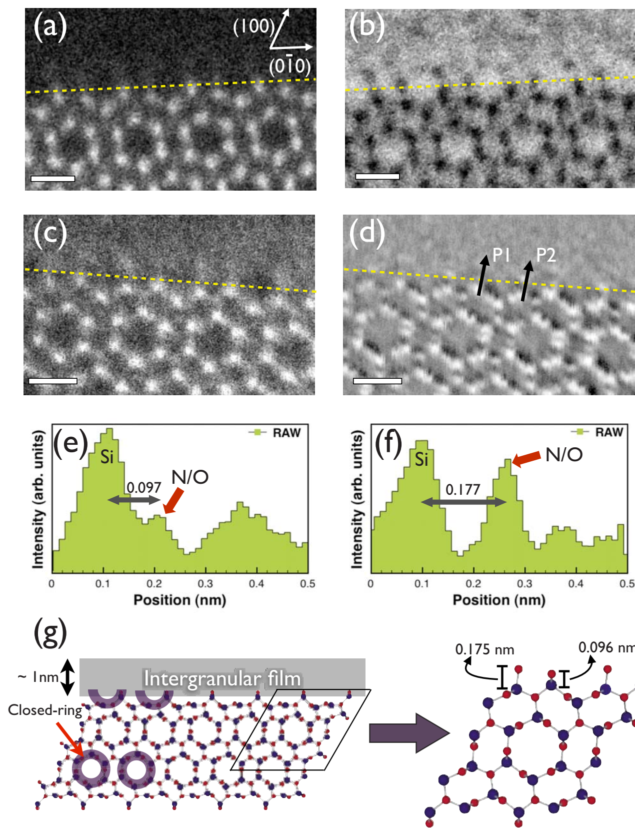

FIG. 1. (Color online) Atomic-resolution images (raw data), intensity profiles and a schematic of a typical Si_3N_4-SiO_2 interface. The yellow (bright) dotted line in the images marks the interface between the Si_3N_4 grain and the amorphous SiO_2 film. (a) and (b) show simultaneous Z-contrast and annular bright-field images taken at 120 kV. (c) and (d) show simultaneous Z-contrast and bright-field (contrast inverted) images taken at 300 kV. (e) and (f) show the intensity profiles taken at positions (P1) and (P2) as marked in (d), respectively. (g) Schematic of the Si_3N_4 $(10\bar{1}0)$ prismatic plane in the presence of the IGF film. The Si atoms are represented with blue (dark) circles and the N atoms are shown in red (brighter circles). In bulk Si_3N_4 along the [0001] crystallographic orientation, the Si and N atoms form distinct hexagonal structures highlighted by the semitransparent purple rings. Scale bar is 0.5 nm.

kV taken with an aberration-corrected FEI Titan S 80–300 (S)TEM with the spatial resolution of ~0.08 nm. Similarly to the previous images, the presence of the atomic ordering in the amorphous region is clearly visible and matches that seen at 120 kV. These results suggest that the observed arrangement is not induced by the high-energy electron beam in the experiment, but it is formed during the microstructural evolution of the ceramic at the crystal/amorphous boundaries. The projected 2-dimensional distances from the Si atoms in the terminating rings to the nearest neighbors in the IGF are approximately (0.097 ± 0.016 nm) and (0.177 ± 0.016 nm) as shown by the intensity profiles in Figs. 1(e) and 1(f), corresponding to positions (P1) and (P2) in Fig. 1(d), respectively. These distances fall in the range of the Si-N and Si-O bond length measurements for the bare and oxygenated Si_3N_4 surfaces,[21,22] suggesting that the observed atomic arrangements could involve either N and/or O

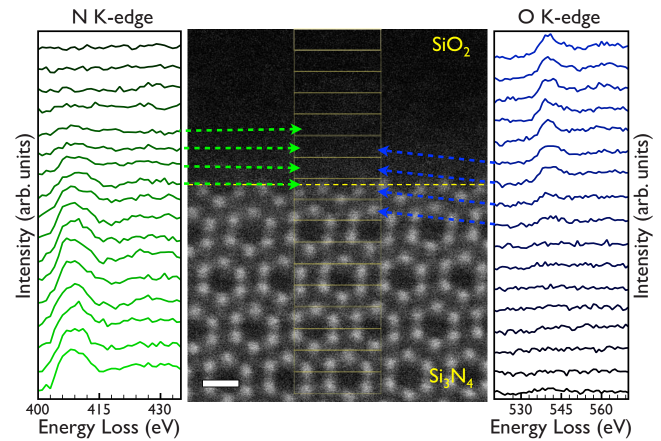

FIG. 2. (Color online) Z-contrast image (raw data) of the Si_3N_4/SiO_2 interface (middle) and the N *K* and O *K* edges (sides) extracted from the area scans. The yellow (bright) rectangles on the Z-contrast image highlight the individual scan-areas (horizontal length is not shown at scale but is for illustrative purposes only). Each spectrum gives the average information of the rectangular area of 5.48×0.27 nm^2. Scale bar is 0.5 nm.

atoms, i.e., the observed structures in the amorphous IGF could be partially oxygenated. It is also important to point out that these interfacial structures resemble the theoretically predicted *closed-ring* $(10\bar{1}0)$ surface of Si_3N_4,[21] as shown schematically in the bottom portion of Fig. 1(g). Although structurally similar, the observed structures in the SiO_2 region are not those of Si_3N_4 closed-ring termination since they are slightly distorted from the ideal closed-ring geometry and they are missing the closing atom at the top of the ring. To identify the composition of the observed structures we carried out atomically-resolved EELS experiments along and across the interface.

First, we performed spatially resolved EELS at 300 keV using a dedicated aberration-corrected VG 603 STEM. To minimize radiation dose, the spectra were collected by rastering the electron beam over a rectangular area of 5.48 $\times 0.27$ nm^2 for 0.5 s.[23] Figure 2 shows the acquired O *K* and N *K* edges along with the Z-contrast image indicating the regions of the area scans. Each of the spectra corresponds to the signal enclosed by the corresponding rectangle superimposed on the image, and it provides the average information of the enclosed area. The spectra reveal that O is present at the surface and the subsurface of Si_3N_4 as the O *K*-edge signal remains strong ~0.54 nm into the bulk of Si_3N_4. On the other hand, the N *K*-edge signal is prominent in the SiO_2 IGF close to the interface. These results are consistent with O replacing N in Si_3N_4 as shown earlier.[22]

Next, we performed atomic-resolution Spectrum Imaging (SI) in EELS using the JEOL ARM 200F by scanning the focused electron-probe in a raster of pixels while collecting a spectrum at each pixel. The acquisition time of each pixel was 0.05 s. We note here that the atomic-resolution EELS was acquired at 80 kV at the Si_3N_4 crystal/amorphous interfaces. Figure 3 shows the Si L_{23} edges taken from six different positions in the Si/N terminating ring as extracted from the SI data. These positions correspond to the Si sites in the

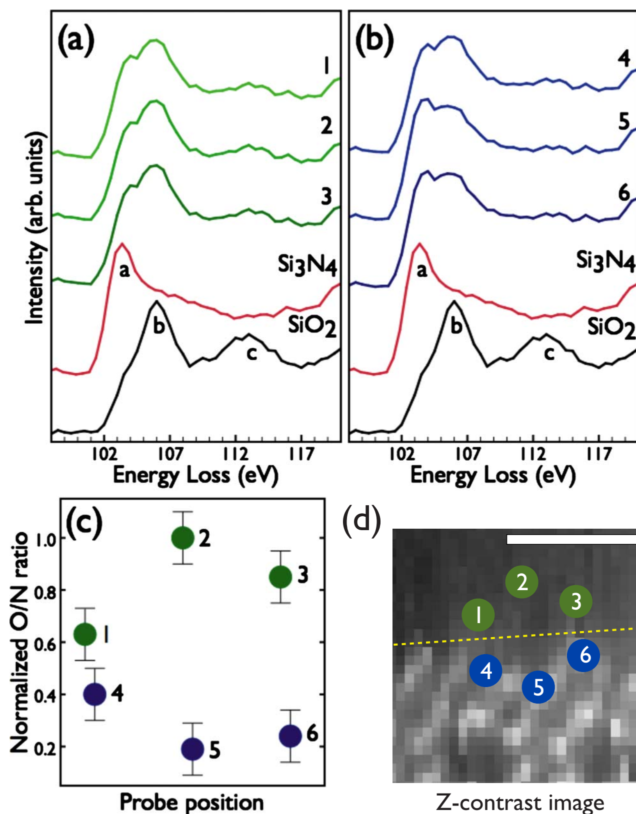

FIG. 3. (Color online) (a) and (b) show the Si L-edge taken at the Si_3N_4 and SiO_2 interface at six different positions shown in the simultaneously acquired Z-contrast image (d). The Si L edges from bulk Si_3N_4 and SiO_2 are also shown for comparison. (c) shows the integrated O/N ratios at the six positions (normalized with respect to their maximum, position 2) acquired from N and O signals. Scale bar in (d) is 0.5 nm. The shown EEL spectra have been background subtracted and correspond to the sum of four neighboring-pixels in the SI data set.

bulk of Si_3N_4. For comparison, the Si L-edges from bulk Si_3N_4 and SiO_2 are also shown and can be used to identify the bonding characteristics of the interfacial Si atoms. By examining the spectra one can see that the Si signals at all six positions present both Si-N and Si-O bonding features (all six spectra show peaks a, b, and c of the Si_3N_4 and the SiO_2 reference spectra). However, the spectra at positions 1, 2, 3, and 4 show stronger Si-O bonding features than those of positions 5 and 6 since their peaks at 105 eV (labeled as b on the SiO_2 reference spectra) are more pronounced.

It is also interesting to note that the Si signals at positions 4 and 6, representing the two ends of the terminating open-ring, have slightly different features, thus distinct bonding characteristics. To investigate this observation further, we looked at the O and N signals acquired simultaneously with the Si L_{23} edge. Due to their smaller signal-to-noise-ratio as compared to the Si signal, the extraction of N and O bonding characteristics was not possible from their respective edges. Nevertheless, by integrating these signals over 40 eV energy window and by taking into account the corresponding inelastic cross-sections, elemental ratios of O/N concentrations were computed[24] at each of the six positions. Figure 3(c) shows these ratios normalized with respect to their maximum, i.e., position 2. As noted previously, the calculated ratios are different at the two ends of the terminating Si_3N_4 open-ring (positions 4 and 6), suggesting a compositional asymmetry at the Si_3N_4 surface. Note that this difference is not caused by beam broadening because the distance between 1 and 4 is the same as the separation between 3 and 6, but 3 and 6 show the highest compositional changes. This can only be explained by site specific intermixing across the interface. Moreover, in agreement with the EELS results at 300 kV, the largest O/N ratio was found for the atomic columns deeper into the SiO_2 film (position 2), while the smallest was obtained in the Si_3N_4 region. Both results indicate that the N and O atoms order across as well as along the interface with a slight asymmetry.

In summary, we have presented results on and analyses of the interface between crystalline Si_3N_4 grains and amorphous SiO_2 film using a combination of STEM imaging techniques and atomically-resolved EELS. The STEM images reveal the presence of crystalline atomic structures past the interface and into the amorphous SiO_2. A detailed analysis of the images indicates that Si, N, and O atoms arrange in SiO_2 in ways resembling the crystalline structure of Si_3N_4. We also find that there is a nonuniform interatomic mixing of oxygen and nitrogen at different atomic sites in the interface with the O atoms replacing N at the surface and subsurface of Si_3N_4. The presented results have important consequences for the properties of crystal/amorphous interfaces in Si_3N_4, especially in regards to interface strength. The substitution of O for N decreases the coordination number of the interfacial Si atoms since N bonds to three Si atoms whereas O bonds two Si atoms. This, in turn, may promote weakening of the interface[2,25] and facilitate debonding and an intergraular crack propagation. The results have important implications for understanding Si_3N_4 surfaces and their interactions with amorphous IGFs. The information about the specific atomic structure and bonding characteristics at the interfaces between Si_3N_4 and the IGFs composed of light elements, always present in Si_3N_4, should aid in understanding how ceramic microstructures evolve during sintering processes and enable detailed computer simulations of structures and properties. The ability to control the atomic evolution of the interfaces, in turn, can help in the improvement of the Si_3N_4 properties and performance in a wide-range of applications.[26–28]

The work was supported by the NSF under Grant No. DMR-0605964 (W.W., R.F.K., and J.C.I.), DOE grant DE-F002-09ER46554 (S.T.P.), the Office of Basic Energy Sciences, Materials Sciences and Engineering Division, U.S. Department of Energy (S.J.P. and S.T.P.), the SHaRE User Facility (J.C.I.), which is sponsored by the Scientific User Facilities Division, Office of Basic Energy Sciences, U.S. Department of Energy, and by the McMinn Endowment (S.T.P.) at Vanderbilt University. S.O. acknowledges support by the National Science Foundation under the Independent Research/Development program while working at the Foundation.

[1] R. W. Cahn, P. Hassen, and E. J. Kramer, *Materials Science and Technology*, Structure and Properties of Ceramics (Wiley-VCH, Weinheim, 1994), p. 751.
[2] P. F. Becher, G. S. Painter, E. Y. Sun, C. H. Hsueh, and M. J. Lance, Acta Mater. **48**, 4493 (2000).
[3] M. J. Hoffmann and G. Petzow, *Tailoring of Mechanical Properties of* Si_3N_4 *Ceramics*, NATO ASI Series E, Applied Sciences Vol. 276 (Kluwer Academic, Dordrecht, 1994).
[4] R. L. Satet and M. J. Hoffmann, J. Am. Ceram. Soc. **88**, 2485 (2005).
[5] R. L. Satet, M. J. Hoffmann, and R. M. Cannon, Mater. Sci. Eng., A **422**, 66 (2006).
[6] P. F. Becher, G. S. Painter, N. Shibata, R. L. Satet, M. J. Hoffmann, and S. J. Pennycook, Mater. Sci. Eng. A **422**, 85 (2006).
[7] P. F. Becher, G. S. Painter, N. Shibata, S. B. Waters, and H.-T. Lin, J. Am. Ceram. Soc. **91**, 2328 (2008).
[8] N. Shibata, G. S. Painter, P. F. Becher, and S. J. Pennycook, Appl. Phys. Lett. **89**, 051908 (2006).
[9] N. Shibata, S. J. Pennycook, T. R. Gosnell, G. S. Painter, W. A. Shelton, and P. F. Becher, Nature (London) **428**, 730 (2004).
[10] A. Ziegler, J. C. Idrobo, M. K. Cinibulk, C. Kisielowski, N. D. Browning, and R. O. Ritchie, Science **306**, 1768 (2004).
[11] G. B. Winkelman, C. Dwyer, T. S. Hudson, D. Nguyen-Manh, M. Döblinger, R. L. Satet, M. J. Hoffmann, and D. J. H. Cockayne, Philos. Mag. Lett. **84**, 755 (2004).
[12] A. Ziegler, J. C. Idrobo, M. K. Cinibulk, C. Kisielowski, N. D. Browning, and R. O. Ritchie, Appl. Phys. Lett. **88**, 041919 (2006).
[13] G. B. Winkelman, C. Dwyer, C. Marsh, T. S. Hudson, D. Nguyen-Manh, M. Döblinger, and D. J. H. Cockayne, Mater. Sci. Eng., A **422**, 77 (2006).
[14] K. van Benthem, G. S. Painter, F. W. Averill, S. J. Pennycook, and P. F. Becher, Appl. Phys. Lett. **92**, 163110 (2008).
[15] W. Walkosz, R. F. Klie, S. Öğüt, A. Borisevish, P. F. Becher, S. J. Pennycook, and J. C. Idrobo, Appl. Phys. Lett. **93**, 053104 (2008).
[16] S. H. Garofalini and W. W. Luo, J. Am. Ceram. Soc. **86**, 1741 (2003).
[17] J. Chen, L. Ouyang, P. Rulis, A. Misra, and W. Y. Ching, Phys. Rev. Lett. **95**, 256103 (2005).
[18] M. Yoshiya, K. Tatsumi, I. Tanaka, and H. Adachi, J. Am. Ceram. Soc. **85**, 1 (2002).
[19] W. Y. Ching, P. Rulis, L. Ouyang, S. Aryal, and A. Misra, Phys. Rev. B **81**, 214120 (2010).
[20] T. Marten, E. I. Isaev, B. Alling, L. Hultman, and I. A. Abrikosov, Phys. Rev. B **81**, 212102 (2010).
[21] J. C. Idrobo, H. Iddir, S. Öğüt, A. Ziegler, N. D. Browning, and R. O. Ritchie, Phys. Rev. B **72**, 241301 (2005).
[22] W. Walkosz, J. C. Idrobo, R. F. Klie, and S. Öğüt, Phys. Rev. B **78**, 165322 (2008).
[23] T. Zheleva, A. Lelis, G. Duscher, F. Liu, I. Levin, and M. Das, Appl. Phys. Lett. **93**, 022108 (2008).
[24] R. F. Egerton, *Electron Energy Loss Spectroscopy in the Electron Microscope* (Plenum, New York, 1996).
[25] S. Veprek, P. Karvankova, and M. G. J. Veprek-Heijman, J. Vac. Sci. Technol. B **23**, L17 (2005).
[26] M. H. White, D. A. Adams, and J. Bu, IEEE Circuits Devices Mag. **16**, 22 (2000).
[27] L. Liu, J. P. Xu, L. L. Chen, and P. T. Lai, Microelectron. Reliab. **49**, 912 (2009).
[28] A. Kaźmierczak, F. Dortu, O. Schrevens, D. Giannone, L. Vivien, D. Marris-Morini, D. Bouville, E. Cassan, K. B. Gylfason, H. B. Sohlström, B. Sanchez, A. Griol, and D. Hill, Opt. Eng. **48**, 014401 (2009).